ADVANCED MATERIALS

calculated from the oxidation potential versus the internal standard of ferrocene/ferrocenium and the I_p (5.43 eV) so obtained for PATPD was in good agreement with the I_p reported for TPD based materials (5.4 eV determined by UV-PES) [26].

Absorption Spectra: Absorption spectra of the samples were measured with a Cary 5G spectrophotometer.

Dark Conductivity and Photoconductivity: Steady-state conductivity properties were determined in the dark. To measure the steady-state dark conductivity, an electric field (E_a) was applied and the current (i_{dark}) was measured. To assure steady-state conditions a dwell time of 15 s between each reading was used. The applied electric field was swept from 0 to 76 V μm^{-1} over a period of 7 min. The current was measured using a Keithley 6517A electrometer.

Four-Wave Mixing and Exposure Dependent Transient Four-Wave Mixing Experiments: A detailed discussion about the experimental set-up is given in [22].

Received: January 23, 2004
Final version: June 8, 2004

[1] F. Würthner, S. Yao, J. Schilling, R. Wortmann, M. Redi-Abshiro, E. Mecher, F. Gallego-Gomez, K. Meerholz, *J. Am. Chem. Soc.* **2001**, *123*, 2810.
[2] D. Wright, U. Gubler, Y. Roh, W. E. Moerner, M. He, R. J. Tweig, *Appl. Phys. Lett.* **2001**, *79*, 4274.
[3] L. Solymar, D. J. Webb, A. Grunnet-Jepsen, *The Physics and Applications of Photorefractive Materials*, Clarendon, Oxford, UK **1996**.
[4] B. Kippelen, S. R. Marder, E. Hendrickx, J. L. Maldonado, G. Guillemet, B. L. Volodin, D. D. Steele, Y. Enami, Sandalphon, Y. J. Yao, J. F. Wang, H. Röckel, L. Erskine, N. Peyghambarian, *Science* **1998**, *279*, 54.
[5] E. Mecher, F. Gallego-Gómez, H. Tillmann, H. H. Hörhold, J. C. Hummelen, K. Meerholz, *Nature* **2002**, *418*, 959.
[6] E. Hendrickx, Y. Zhang, K. B. Ferrio, J. A. Herlocker, J. Anderson, N. R. Armstrong, E. A. Mash, A. P. Persoons, N. Peyghambarin, B. Kippelen, *J. Mater. Chem.* **1999**, *9*, 2251.
[7] K. Meerholz, R. Bittner, Y. De Nardin, C. Bräuchle, E. Hendrickx, B. L. Volodin, B. Kippelen, N. Peyghambarian, *Adv. Mater.* **1997**, *9*, 1043.
[8] A. Grunnet-Jepsen, D. Wright, B. Smith, M. S. Bratcher, M. S. DeClue, J. S. Siegel, W. E. Moerner, *Chem. Phys. Lett.* **1998**, *291*, 553.
[9] J. A. Herlocker, C. Fuentes-Hernandez, K. B. Ferrio, E. Hendrickx, P.-A. Blanche, N. Peyghambarian, B. Kippelen, Y. Zhang, J. F. Wang, S. R. Marder, *Appl. Phys. Lett.* **2000**, 77, 2292.
[10] O. Ostroverkhova, K. D. Singer, *J. Appl. Phys.* **2002**, *92*, 1727.
[11] M. Barzoukas, M. Blanchard-Desce, *J. Chem. Phys.* **2000**, *112*, 2036.
[12] K. Meerholz, B. L. Volodin, Sandalphon, B. Kippelen, N. Peyghambarian, *Nature* **1994**, *371*, 497.
[13] A. Grunet-Jepsen, C. L. Thompson, W. E. Moerner, *Science* **1997**, *277*, 549
[14] K. Ogino, T. Nomura, T. Schichi, S. H. Park, H. Sato, T. Aoyama, T. Wada, *Chem. Mater.* **1997**, *9*, 2768.
[15] J. Cornil, N. E. Gruhn, D. A. dos Santos, M. Malagoli, P. A. Lee, S. Barlow, S. Thayumanavan, S. R. Marder, N. R. Armstrong, J.-L. Brédas, *J. Phys. Chem. A* **2001**, *105*, 5206.
[16] R. D. Miller, V. Y. Lee, R. J. Twieg, *J. Chem. Soc. Chem. Commun.* **1995**, 245.
[17] A. Yamamori, C. Adachi, T. Koyama, Y. J. Taniguchi, *J. Appl. Phys.* **1999**, *86*, 4369.
[18] K. Staub, G. A. Levina, S. Barlow, T. C. Kowalczyk, H. S. Lackritz, M. Barzoukas, A. Fort, S. R. Marder, *J. Mater. Chem.* **2003**, *13*, 825.
[19] S. R. Marder, B. Kippelen, A. K.-Y. Jen, N. Peyghambarian, *Nature* **1997**, *388*, 845.
[20] K. Meerholz, Y. D. Nardin, R. Bittner, R. Wortmann, F. Würthner, *Appl. Phys. Lett.* **1998**, *73*, 4.
[21] C. A. Reed, R. D. Bolskar, *Chem. Rev.* **2000**, *100*, 1075.
[22] C. Fuentes-Hernandez, J. Thomas, R. Termine, M. Eralp, M. Yamamoto, K. Cammack, K. Matsumoto, G. Meredith, N. Peyghambarian, B. Kippelen, S. R. Marder, *Proc. SPIE-Int. Soc. Opt. Eng.* **2003**, *5216*, 83.
[23] U. Hofmann, M. Grasruck, A. Leopold, A. Schreiber, S. Schloter, C. Hohle, P. Strohriegl, D. Haarer, S. J. Zilker, *J. Phys. Chem B* **2000**, *104*, 3887.
[24] D. Wright, M. A. Diaz-Garcia, J. D. Casperson, M. DeClue, W. E. Moerner, R. Twieg, *Appl. Phys. Lett.* **1998**, *73*, 1490.
[25] L. Wang, M. K. Ng, L. Yu, *Appl. Phys. Lett.* **2001**, *78*, 700.
[26] J. D. Anderson, E. M. McDonald, P. A. Lee, M. L. Anderson, E. L. Ritchie, H. K. Hall, T. Hopkins, E. A. Mash, J. Wang, A. Padias, S. Thayumanavan, S. Barlow, S. R. Marder, G. Jabbour, S. Shaheen, B. Kippelen, N. Peyghambarian, R. M. Wightman, N. R. Armstrong, *J. Am. Chem. Soc.* **1998**, *120*, 9646.

Carbon-Nanotube-Reinforced Polymer-Derived Ceramic Composites**

By *Linan An*,* *Weixing Xu*, *Sudhir Rajagopalan*, *Chongmin Wang*, *Hsin Wang*, *Yi Fan*, *Ligong Zhang*, *Dapeng Jiang*, *Jay Kapat*, *Louis Chow*, *Baohua Guo*, *Ji Liang*, and *Raj Vaidyanathan*

Carbon nanotubes (CNTs) have attracted tremendous interest in the last decade because of their superior properties. Theoretical and experimental studies have shown that single-walled carbon nanotubes (SWCNTs) possess Young's moduli

[*] Prof. L. An, W. Xu, S. Rajagopalan, Prof. J. Kapat, Prof. L. Chow, Prof. R. Vaidyanathan
Advanced Materials Processing and Analysis Center
Mechanical, Materials and Aerospace Engineering Department
University of Central Florida
Orlando, FL 32816 (USA)
E-mail: lan@mail.ucf.edu
Dr. C. Wang
Pacific Northwest National Laboratory
902 Battelle Boulevard
Richland, WA 99352 (USA)
Dr. H. Wang
High Temperature Materials Laboratory
Oak Ridge National Laboratory
One Bethel Valley Rd., Oak Ridge, TN 37831 (USA)
Dr. Y. Fan, Dr. L. Zhang, Dr. D. Jiang
Laboratory of Excited State Process
Changchun Institute of Optics, Fine Mechanics and Physics
Chinese Academy of Sciences
Changchun 130022, Jilin Province (P. R. China)
Prof. B. Guo, Prof. J. Liang
Chemistry Department,
Tsinghua University
Beijing 106084 (P. R. China)

[**] The TEM work was performed at the EMSL, a national scientific user facility sponsored by DOE's Office of Biological and Environmental Research and located at Pacific Northwest National Laboratory, operated for DOE by Battelle. This work was partially supported by the "Hundred Person" Program of the Chinese Academy of Sciences.

  DOI: 10.1002/adma.200306241

of the order of 1–5 TPa[1–4] and tensile strengths as high as 60 GPa.[5,6] Depending on their diameters and orientations of their hexagons with respect to their tube axes, CNTs can be either semiconducting or metallic.[7,8] The axial thermal conductivity of CNTs is higher than even that of diamond.[9] These unique properties suggest that CNTs hold great promise for synthesizing new kinds of multifunctional nanocomposites. As for their use in ceramic-matrix composites, at least two different architectures can be conceived: i) CNTs can be used as reinforcements to improve mechanical properties and add new functionality, and ii) ceramic matrices can be used to protect functional CNT structures from harsh environments. The ceramic-matrix composites are potentially important for those applications where requirements such as mechanical strength or resistance to corrosive environments prevent the use of other matrices such as polymers and metals. CNT–ceramic composites have been the subject of several previous investigations. Ma et al. synthesized SiC composites containing 10 vol.-% of multiwalled carbon nanotubes (MWCNTs) by hot-pressing a mixture of nanometer-sized ceramic powders and CNTs.[10] Similar processing was used by Siegel et al. to produce MWCN–Al_2O_3 composites.[11] Peigney and co-workers synthesized CNT–Fe/Al_2O_3 composites by growing either SWCNTs or MWCNTs in situ.[12–16] However, only slight improvements in mechanical properties were observed in these previous studies. More recently, Zhan et al. reported the synthesis of nano-phased Al_2O_3 composites containing SWCNTs by a spark-plasma sintering (SPS) technique; the composites possessed significantly improved mechanical properties[17] and electrical conductivity over the pure matrix materials.[18]

The effective utilization of CNTs in composites depends strongly on the ability to disperse nanotubes homogeneously throughout the matrix and to achieve strong interfacial bonding between the CNTs and the matrix in order to ensure load translation. These requirements are difficult to achieve with conventional powder-based ceramic processing techniques. In this communication, we report for the first time on the synthesis of CNT-reinforced ceramic composites by using polymer-derived ceramics (PDCs). Unlike conventional ceramics obtained by sintering powders, PDCs are synthesized by direct thermal decomposition of polymeric precursors,[19,20] which can be in either liquid form, melt form, or organic solution. This unique chemical-to-ceramic technique is particularly suitable for the fabrication of CNT-reinforced (or other reinforced) ceramic composites, since the desired dispersion of CNTs can be rather easily achieved in liquid-phase precursors just prior to pyrolysis. It is also possible to control the ceramic–CNT interfacial properties by modifying either the surface of the CNTs or the chemistry of the precursors, or both.

In this study, two composites containing different amounts of MWCNTs were synthesized using commercially available liquid-phase polyurea(methylvinyl)silazane (CERASET, KiON, US) as a precursor, and a pressure-assisted pyrolysis technique.[21] For comparison, a monolithic ceramic without CNT additives was also synthesized under the same processing conditions, using only CERASET. A previous study[22] demonstrated that under the processing conditions used in this work, CERASET was converted to the fully dense amorphous silicon carbonitride (SiCN) ceramic, with an apparent composition of $SiC_{0.99}N_{0.85}$; the final ceramic also contained ~0.8 wt.-% of residual hydrogen. Thermal gravimetric analysis (TGA) revealed that the pyrolysis resulted in a weight loss of ~30 wt.-% of the original weight of the CERASET, accompanied by a linear shrinkage of ~28 %. The composites and the monolithic ceramic showed the same amount of shrinkage, suggesting that the addition of CNTs was not detrimental to the densification process. This is because CNTs are flexible and thus exhibit little restriction on the matrix shrinkage associated with pyrolysis. The final densities of the composites and the monolithic SiCN were measured and are listed in Table 1. By taking into account the weight loss, using the density of monolithic SiCN as that of the matrix, and the density of graphite (2.25 g cm^{-3}) as that of the MWCNTs, the volume-fractions of the MWCNTs in the final ceramic composites were calculated and are also included in Table 1. The theoretical densities of the composites were then calculated according to the rule of mixtures. The relative densities of the composites were also calculated and are tabulated in Table 1 as well. Both composites had relative densities that were 99 % of their theoretical densities.

Table 1. Properties of CNT-reinforced PDC composites (TD: theoretical density).

	Density [g cm^{-3}]	Relative density [% TD]	Young's modulus [GPa]	Hardness [GPa]
SiCN	2.08	–	74	9.4
SiCN-1.3 vol.–% CNT	2.06	99	109	10.5
SiCN-6.4 vol.–% CNT	2.06	99	118	14.3

Scanning electron microscopy (SEM) observations of the composites and the monolithic ceramic did not reveal defects in any of the specimens and the micrographs (not shown) were featureless (no contrast between the MWCNTs and SiCN), confirming their very dense structure. To assess the distribution of the nanotubes in the ceramic matrix, fracture surfaces of the composites were investigated using SEM. A representative SEM image of a fracture surface of the composite containing 6.4 vol.-% MWCNTs is shown in Figure 1. As can be seen from the image, the nanotubes are uniformly distributed in the ceramic matrix. The image also reveals substantial nanotube pullout from the ceramic matrix with an average pullout length of 5 to 10 μm. Although the bonding between CNTs and polymer-derived ceramics is very strong,[23] the high tensile strength and flexibility of CNTs allow pullout to occur. This result suggests that the composites may possess a significantly high fracture toughness due to nanotube bridging. Further characterization of the microstructure of the composites was carried out by high-resolution transmission electron microscopy (HRTEM). Figure 2 is a

ADVANCED MATERIALS

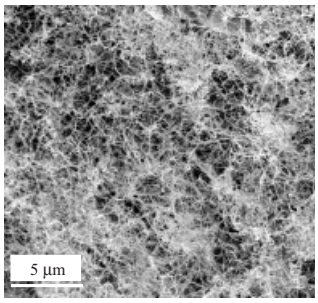

Figure 1. SEM image of the fracture surface of a CNT–SiCN composite containing 6.4 vol.-% MWCNTs.

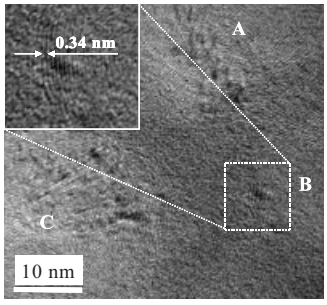

Figure 2. HRTEM image of a CNT–SiCN composite containing 6.4 vol.-% MWCNTs. Three MWCNTs can be seen from the image as indicated by A, B, and C. The fringe spacing of 0.34 nm is typical of graphite, suggesting the images were indeed of MWCNTs.

representative HRTEM image of the composite containing 6.4 vol.-% MWCNTs. The image reveals that the integrity of the CNTs is retained and that the interfaces between the CNTs and the matrix are clean, indicating no reaction between the CNTs and the matrix. This result clearly demonstrates that the MWCNTs can survive the pyrolysis and the associated generation of gaseous by-products such as NH_3, H_2, and CH_4.[24] The lack of any reaction between the gases and MWCNTs may be due to the fact that the gases were released at relatively low temperatures.[24]

Mechanical behavior of the composites was investigated using instrumented nano-indentation.[25] Qualitative studies using a sharp, diamond Berkovich tip (nominal tip radius: 50 nm) was carried out on the composites. No "pop-ins", or steps in the load–depth response, indicative of a porous matrix, were observed. To assess their elastic–plastic deformation behavior, indentation-load–displacement (P–h) curves were measured using a spherical diamond indenter, 100 μm diameter, for both the composites and the monolithic ceramics. The results are summarized in Figure 3. The inset is a magnification of the residual deformation associated with each of the specimens. The indentation results indicate that the stiffness of the composites increased with increasing CNT content. More significantly, the residual deformation decreases with increasing CNT content—in particular, the composite containing 6.4 vol.-% CNTs showed almost no residual deformation, suggesting remarkable improvement in contact-damage resistance. This result is rather surprising since the P–h curve of the 6.4 vol.-% CNT composite clearly shows "plastic" deformation (displacement–load curve deviates from Hertzian elastic behavior[26]). The possible explanation is that the cone cracks formed under Hertzian indentation[26] were bridged by partially debonded CNTs that deformed elastically. When the applied load was withdrawn, the elastic restoration of the CNTs exerted a closing force on the cracks to restore the deformed material. Further investigation into this issue is ongoing. This result suggests that the composite may possess a significantly high fatigue resistance under localized cycling loads.

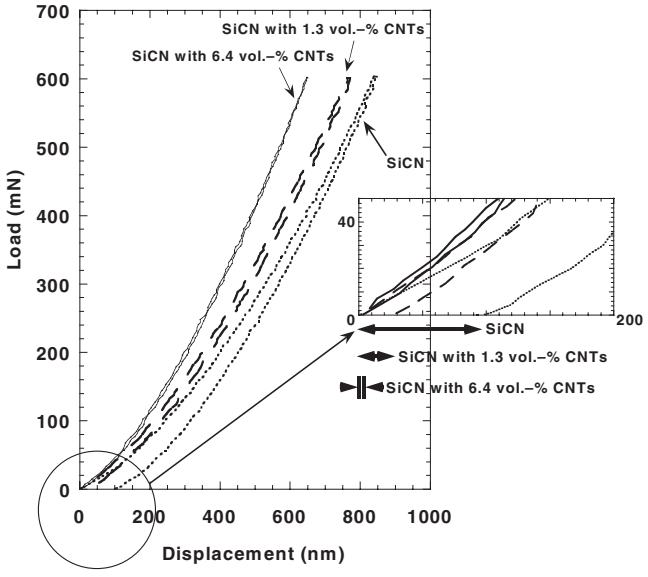

Figure 3. Load–displacement curves measured using a spherical diamond indenter (radius 50 μm) for a 6.4 vol.-% CNT composite, 1.3 vol.-% CNT composite, and monolithic SiCN. The inset is a magnification of the bottom left corner, which shows the permanent deformation formed on unloading.

The Young's moduli (E-moduli) were calculated from the nanoindentation curves for the composites and monolithic SiCN; the results are listed in Table 1 and plotted in Figure 4

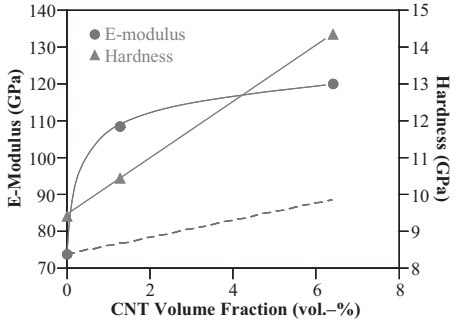

Figure 4. Variation of the Young's modulus and hardness with CNT volume fraction in SiCN–CNT composites. The dashed line is the predicted modulus calculated from an existing model (Eq. 1), which significantly underestimates the measured values.

as a function of CNT content. It can be seen that the E-modulus increased significantly with increasing CNT content; and an increase of over 150 % was achieved with only 6.4 vol.-% added CNTs. The relatively low E-modulus for the monolithic SiCN could have been due to the existence of residual hydrogen. It is instructive to compare experimental results with calculations from a theoretical model. This was accomplished by modeling the composites as randomly oriented, discontinuous fiber composites. By assuming that the CNTs bonded strongly to the matrix and allowing for load transfer from the matrix to the CNTs through interfacial shear stress, a Young's modulus for the composite, E_c, was calculated using the Halpin–Tsai equation:[27]

$$E_c = \left[\frac{3(1+2(l/d)\eta_L V_f)}{8(1-\eta_L V_f)} + \frac{5(1+2\eta_T V_f)}{8(1-\eta_T V_f)}\right] E_m \quad (1)$$

where

$$\eta_L = \frac{(E_{CNT}/E_m)-1}{(E_{CNT}/E_m)+2(l/d)} \quad (2)$$

and

$$\eta_T = \frac{(E_{CNT}/E_m)-1}{(E_{CNT}/E_m)+2} \quad (3)$$

E_{CNT} and E_m are the moduli for the CNT and ceramic matrix, respectively, L is the length, d is the outer diameter, and V_f is the volume percentage of the nanotubes. The Young's modulus of MWCNTs is known to be strongly dependent on their diameters[3,5,28–30] and exhibits a range of values. We have chosen to use a modulus of 450 GPa, as reported by Wong et al.,[28] since it is a representative, mid-range value. The moduli were calculated from Equation 1 and are shown in Figure 4 as a dashed line. It can be seen that Equation 1 significantly underestimates the moduli of the composites. The underlying mechanism that causes the discrepancy between the experimental and theoretical results is not clear at present. The residual stress due to the large shrinkage associated with pyrolysis could play a key role in the improvement of the E-modulus. The hardness of the three materials was measured using microindentation and is reported in Table 1 and Figure 4. The hardness increased linearly with CNT content; an increase in hardness of over 150 % was achieved with only 6.4 vol.-% added CNTs. Again, the relatively low value of hardness for the monolithic SiCN can be ascribed to the presence of hydrogen.

In summary, fully dense ceramic–CNT composites with homogeneously distributed MWCNTs have been synthesized by using polymer-derived ceramics as matrices. The nanotubes retained their integrity during the polymer–ceramic conversion and exhibited strong pullout from the ceramic matrix. The mechanical properties, such as E-modulus, hardness, and damage resistance, of the composites were significantly increased by adding only 6.4 vol.-% CNTs. The present work suggests a new way to synthesize ceramic–CNT composites with improved properties.

Experimental

Liquid phase CERASET was used as obtained. Multiwalled carbon nanotubes with an average diameter of ~30 nm and an average length of ~30 μm were provided by Tsinghua University, China. The MWCNTs were first washed with HNO_3 (60 wt.-%) at 60–70 °C for 10 h. SEM observations on the washed CNTs showed that the CNTs retained their original geometry but were less closely packed, and also that metallic catalyst particles and free carbons previously existing in the as-received nanotubes were effectively removed. The acid-washed nanotubes were then treated with aniline by mixing the CNTs and aniline in acetone under high-energy sonication (100 W). A previous study demonstrated that aniline can enhance the dispersion of nanotubes in polymer matrices [31]. Excess aniline was then removed by repeatedly washing with de-ionized water. After drying, the CNTs were mixed with liquid CERASET using high-energy sonication for ~0.5 h, followed by magnetic stirring for 24 h, to form a CNT-containing suspension. 3 wt.-% of dicumyl peroxide (Acros Organics, NJ, USA) was also added to the suspension to lower the solidification temperature of CERASET [32,33]. No CNT sedimentation was observed after setting the suspension for 48 h, which was the first indication that the nanotubes were homogeneously dispersed in the CERASET. Two suspensions were prepared, containing 1 and 5 wt.-% CNTs. The suspensions were then converted to dense ceramic–CNT composites by pressure-assisted pyrolysis [21]. First, the suspension was poured into a Teflon tube with an inner diameter of 12.5 mm, and then it was solidified by heat-treating at 150 °C for 15 min. The solid rod obtained was then crosslinked at 400 °C in N_2, under an isostatic pressure of 30 MPa. Discs of 2–3 mm thickness were cut from the rod and pyrolysized at 1000 °C in N_2, under a pressure of 30 MPa. For comparison, the monolithic SiCN discs were prepared under the same conditions using pure CERASET.

The weight loss during pyrolysis was measured using TGA. The densities of both composites and the monolithic SiCN were measured using Archimedes' principle. The microstructure of the composites was examined using SEM and HRTEM. The mechanical behavior was investigated by microindentation and instrumented nanoindentation, using a spherical diamond indenter (radius: 50 μm).

Received: September 29, 2003
Final version: March 10, 2004

[1] B. I. Yakobson, C. J. Brabec, J. Bernholc, *Phys. Rev. Lett.* **1996**, *76*, 2511.
[2] G. Van Lier, C. Van Alsenoy, V. Van Doren, P. Geerlings, *Chem. Phys. Lett.* **2000**, *326*, 181.
[3] M. M. J. Treacy, T. W. Ebbesen, J. M. Gibson, *Nature* **1996**, *381*, 678.
[4] O. Lourie, H. D. Wagner, *J. Mater. Res.* **1998**, *13*, 2418.
[5] M. Yu, O. Lourie, M. J. Dyer, K. Moloni, T. F. Kelly, R. S. Ruoff, *Science* **2000**, *287*, 637.
[6] M. Yu, B. S. Files, S. Arepalli, R. S. Ruoff, *Phys. Rev. Lett.* **2000**, *84*, 5552.
[7] N. Hamada, S. I. Sawada, A. Oshiyama, *Phys. Rev. Lett.* **1992**, *68*, 1579.
[8] H. Dai, J. Kong, C. Zhou, N. Franklin, T. Tombler, A. Cassell, S. Fan, M. Chapline, *J. Phys. Chem. B* **1999**, *103*, 11 246.
[9] S. Berber, Y. Kwon, D. Tomanek, *Phys. Rev. Lett.* **2000**, *84*, 4613.
[10] R. Z. Ma, J. Wu, B. Q. Wei, J. Liang, D. H. Wu, *J. Mater. Sci.* **1998**, *33*, 5243.
[11] R. W. Siegel, S. K. Chang, B. J. Ash, J. Stone, P. M. Ajayan, R. W. Doremus, L. S. Schadler, *Scr. Mater.* **2001**, *44*, 2061.
[12] E. Flahaut, A. Peigney, C. Laurent, C. Marliere, F. Chastel, A. Rousset, *Acta Mater.* **2000**, *48*, 3803.
[13] C. Laurent, A. Peigney, O. Dumortier, A. Rousset, *J. Eur. Ceram. Soc.* **1998**, *18*, 2005.
[14] A. Peigney, C. Laurent, O. Dumortier, A. Rousset, *J. Eur. Ceram. Soc.* **1998**, *18*, 1995.

ADVANCED MATERIALS

[15] A. Peigney, C. Laurent, E. Flahaut, A. Rousset, *Ceram. Int.* **2000**, *26*, 677.
[16] A. Peigney, C. Laurent, F. Dobigeon, A. Rousset, *J. Mater. Res.* **1997**, *12*, 613.
[17] G. Zhan, J. D. Kuntz, J. Wan, A. K. Mukherjee, *Nat. Mater.* **2003**, *2*, 38.
[18] G. Zhan, J. D. Kuntz, J. E. Garay, A. K. Mukherjee, *Appl. Phys. Lett.* **2003**, *83*, 1228.
[19] R. Riedel, G. Passing, H. Schonfelder, R. J. Brook, *Nature* **1992**, *355*, 714.
[20] E. Kroke, Y. L. Li, C. Konetschny, E. Lecomte, C. Fasel, R. Riedel, *Mater. Sci. Eng., R* **2000**, *26*, 97.
[21] L. An, W. Zhang, V. M. Bright, M. L. Dunn, R. Raj, in *Proc. of the 13th IEEE Ann. Int. Conf. on Micro Electro Mechanical Systems*, Miyazaki, Japan **2000**, p 619.
[22] L. Bharadwaj, Y. Fan, L. Zhang, D. Jiang, L. An, *J. Am. Ceram. Soc.* **2004**, *87*, 483.
[23] Y. Cai, S. R. Shah, A. Zimmermann, M. Weinmann, R. Rai, F. Aldinger, *Phys. Status Solidi A* **2002**, *193*, R13.
[24] Y. Li, E. Kroke, R. Riedel, C. Fasel, C. Gervais, F. Babonneau, *Appl. Organomet. Chem.* **2001**, *15*, 820.
[25] S. Rajagopalan, R. Vaidyanathan, *JOM* **2002**, *54*, 45.
[26] B. R. Lawn, *J. Am. Ceram. Soc.* **1998**, *81*, 1977.
[27] P. K. Mallick, *Fiber-Reinforced Composites: Materials, Manufacturing and Design*, Marcel Dekker Inc., New York **1993**, p. 130.
[28] E. W. Wong, P. E. Sheehan, C. M. Lieber, *Science* **1997**, *277*, 1971.
[29] P. Poncharal, Z. L. Wang, D. Ugarte, W. A. de Heer, *Science* **1999**, *283*, 1513.
[30] Z. Pan, S. Xie, L. Lu, B. Chang, L. Sun, W. Zhou, G. Wang, D. Zhang, *Appl. Phys. Lett.* **1999**, *74*, 3152.
[31] X. Gong, J. Liu, S. Baskaran, R. D. Voise, J. S. Young, *Chem. Mater.* **2000**, *12*, 1049.
[32] J. M. Schwark, *US Patent 5 032 649*, **1991**.
[33] J. M. Schwark, *US Patent 4 929 704*, **1991**.

High-Efficiency Soft-Contact-Laminated Polymer Light-Emitting Devices with Patterned Electrodes**

By *Tae-Woo Lee*,* *Jana Zaumseil*, *Seong Hyun Kim*, and *Julia W. P. Hsu*

Organic light-emitting diodes (OLEDs) are well-suited for a wide range of existing and future display applications, especially when they are combined with flexible active-matrix circuits that incorporate organic thin-film transistors (OTFTs). OLEDs[1,2] and OTFTs[3] often use metal electrodes deposited directly onto the organic active layers by thermal or electron-beam evaporation or by sputtering.[1–5] In certain cases, this deposition process produces organic/metal interfacial regions characterized by metal in-diffusion and chemical or morphological disruption of the organic region.[4,6,7] Interfaces of this type can adversely affect the device performance, especially for OLEDs, where they potentially introduce quenching centers that can reduce quantum efficiencies and long-term stability. To avoid these problems, inactive buffer layers can be placed between the active organic region and the metal.[4] Our recent work suggests that OLEDs formed by physical lamination of metal electrodes to organic electroluminescent (EL) layers have fewer interfacial quenching sites and better quantum efficiencies than those formed by metal evaporation in vacuum.[8] This soft-contact lamination (ScL) approach relies upon van der Waals' interactions when an EL layer is brought into contact with a thin metal electrode supported by a conformable, elastomeric substrate. Unlike conventional lamination techniques,[9,10] this method does not require applied pressure, heating, or adhesives to establish high-quality electrical contacts. Since this method is inherently compatible with the tools of soft lithography,[11–13] it can be used to produce devices with geometries (i.e., OLED emissive areas or OTFT channel lengths) deep into the submicrometer range.[8,14–17]

Here we describe high-efficiency patterned and unpatterned organic light-emitting devices with Au electrodes by use of ScL with polymer EL layers that are blended with organic salts. Ionic species in polymer light-emitting devices greatly enhance the light intensity and luminous efficiency.[18–21] Expanding on previous work,[18] in which organic ammonium salts were shown to improve the efficiency of multilayer polymer EL devices, we blended the salts directly into the EL polymers. The dipole layers formed by organic salts at the electrode/organic interfaces enhance charge injection and reduce the dependence of device performance on the work function of the electrodes. The resulting devices differ from light-emitting electrochemical cells (LECs)[21] in that the ions are not mobile in organic-salt blend devices, because of the absence of an ion-conducting medium such as poly(ethylene oxide) (PEO). For the work presented here, we use Au as an electrode since it does not form a surface oxide. We compare the luminous efficiency and stability of these devices to those produced in the usual way by thermal evaporation of Au.

Figure 1a schematically illustrates the ScL process. The devices consist of two parts: 1) an elastomeric element of polydimethylsiloxane (PDMS) (shown with a relief structure designed to generate patterned emission) coated with a thin metal film, and 2) a transparent substrate that supports an electrode and an EL organic film. When these two components are brought together, van der Waals' interactions pull them into intimate contact at room temperature without any applied pressure. The resulting contact is mechanically robust, and cannot be peeled apart without additional force. We use the established techniques of soft lithography to form the elastomeric elements. In particular, a pre-polymer of PDMS

[*] Dr. T.-W. Lee, J. Zaumseil, Dr. J. W. P. Hsu
Bell Laboratories, Lucent Technologies
600 Mountain Avenue, Murray Hill, NJ 07974 (USA)
E-mail: taew.lee@samsung.com
Dr. S. H. Kim
Electronics and Telecommunications Research Institute
161 Gajeong-dong, Yuseong-gu, Daejeon 305-350 (Korea)

[**] We thank Dr. Z. Bao, Prof. J. A. Rogers, and Prof. O. O. Park for technical assistance, material support, and helpful comments. We thank Dr. M.-G. Kim for the helpful discussion.

  DOI: 10.1002/adma.200400182